



HAL
open science

A net-exchange Monte Carlo approach to radiation in optically thick systems

A de Lataillade, J. L. Dufresne, Mouna El-Hafi, Vincent Eymet, Richard A Fournier

► **To cite this version:**

A de Lataillade, J. L. Dufresne, Mouna El-Hafi, Vincent Eymet, Richard A Fournier. A net-exchange Monte Carlo approach to radiation in optically thick systems. *Journal of Quantitative Spectroscopy and Radiative Transfer*, 2002, 74 (5), pp.563-584. <10.1016/S0022-4073(01)00272-2>. <hal-01712164>

HAL Id: hal-01712164

<https://hal.science/hal-01712164v1>

Submitted on 22 Mar 2018

HAL is a multi-disciplinary open access archive for the deposit and dissemination of scientific research documents, whether they are published or not. The documents may come from teaching and research institutions in France or abroad, or from public or private research centers.

L'archive ouverte pluridisciplinaire **HAL**, est destinée au dépôt et à la diffusion de documents scientifiques de niveau recherche, publiés ou non, émanant des établissements d'enseignement et de recherche français ou étrangers, des laboratoires publics ou privés.



HAL Authorization

A net-exchange Monte Carlo approach to radiation in optically thick systems

A. de Lataillade^{a,*}, J.L. Dufresne^b, M. El Hafi^a, V. Eymet^c, R. Fournier^c

^a*Centre Energétique-Environnement, UMR CNRS 2392 Ecole des Mines d'Albi-Carmaux,
31 allées des Sciences, 81000 Albi CT, Cedex 09, France*

^b*LMD/CNRS, Université de Paris VI, 75252 Paris, France*

^c*LESETH, Université Paul Sabatier, 31077 Toulouse, France*

Abstract

A Monte Carlo approach to radiative transfer in participating media is described and tested. It solves to a large extent the well known problem of Monte Carlo simulation of optically thick absorption configurations. The approach which is based on a net-exchange formulation and on adapted optical path sampling procedures is carefully designed to insure satisfactory convergence for all types of optical thicknesses. The need for such adapted algorithms is mainly related to the problem of gaseous line spectra representation in which extremely large ranges of optical thicknesses may be simultaneously encountered. The algorithm is tested against various band average computations for simple geometries using the Malkmus statistical narrow band model. © 2002 Elsevier Science Ltd. All rights reserved.

Keywords: Monte Carlo; Sampling optimization; Line spectra; Net-exchange formulations

1. Introduction

Since the emergence of computational physics, Monte Carlo methods have been extensively used for numerical simulation of radiative heat transfer in participating media. They first appeared as strict numerical implementations of photon transport stochastic models [1,2]. As such, they were commonly qualified by “exactness” and were mainly used for production of reference solutions in the process of validating other numerically more efficient simulation techniques.

* Corresponding author. Present address: CERFACS, 42 avenue Gaspard Coriolis, 31057 Toulouse Cedex 01, France.
E-mail address: lataillade@cerfacs.fr (A. de Lataillade).

Recent research efforts depart from this original position in three ways [3,5]:

- (1) underlying physical formulations are intensively rediscussed (reverse formulations, net-exchange formulations), sometimes preserving very little similitude with photon transport models;
- (2) intensive use is made of all available convergence enhancement techniques;
- (3) the emergence of massively parallel hardware allows one to seriously consider statistical methods for operational use (and not only for reference solution production), in particular when thinking of the difficulties encountered with deterministic techniques in front of detailed three-dimensional geometries and complex spectral properties.

Among the strongest handicaps of today's Monte Carlo algorithms, are the difficulties related to numerical behavior in the optically thick limit [4,5]. In case of very short photon mean free paths, most bundles are absorbed in the vicinity of their emission positions which means that only very few bundles effectively participate to distant radiative transfers. The consequence is that Monte Carlo algorithms based on bundle transport formulations require very large numbers of statistical realizations for sufficiently accurate radiative exchange estimations. For less intuitive reasons, as we will illustrate hereafter, path integrated Monte Carlo algorithms encounter similar difficulties.¹

The other numerical difficulty encountered with optically thick media is related to spatial discretization. Computational costs impose constraints to geometrical grid sizes that cannot be reduced sufficiently for the optically thin assumption to be valid. It therefore becomes essential to account for sub-grid scale temperature profiles. In the optically thick limit indeed, the radiative net-exchange between adjacent volumes is proportional to temperature gradients at the interface (diffusion assumption) and the assumption of isothermal meshes would lead to strong energy net-exchange overestimations. This constraint requires that Monte Carlo algorithms do not consider global mesh emissions, starting from mesh boundaries, but instead reduce the physical description to local sub-grid emissions, as a function of sub-grid temperature profiles, through random generations of emission positions [6].

These questions are particularly sensitive in gaseous media as line spectra induce wide ranges of optical thicknesses; the optically thick limit being rapidly encountered in the spectral vicinity of absorption line centers. Solutions were proposed in [4,7,8] to overcome this specific difficulty on the basis of hybrid algorithms, combining Monte Carlo with diffusion algorithms. However, such hybrid algorithms face two new difficulties: that related to the criteria used when switching from one model to the other, and that related to the behavior of diffusion models in the vicinity of surface boundaries. Among recent attempts, Cherkaoui et al. [6,9] showed, for quasi-isothermal H₂O–CO₂–air mixtures, using a narrow band statistical model [10], that thanks to intrinsic reciprocity principle satisfaction, net exchange Monte Carlo algorithms were much less sensitive to optical thickness than standard or reverse Monte Carlo algorithms. However, the spatial integration procedure could not be simply optimized on the basis of average transmission functions. The required computational effort, although much smaller than for standard algorithms, still increased significantly as a function of optical thickness.

¹ In the present text, the terminology “bundle transport algorithm” will be used for algorithms in which energy is distributed via emission of energy bundles, each of which is entirely absorbed at a single stochastically determined location. The alternative terminology “path integrated algorithm” will denote algorithms in which bundle energy is exponentially distributed along stochastically determined semi-infinite optical paths.

We now present such a net exchange Monte Carlo approach devoted to gaseous radiation simulation. Differences with [6] are essentially that:

- spectral integrations are performed with a k -distribution model, randomly generating monochromatic absorption coefficients [11,12] instead of using narrow-band average transmission functions;
- a path integrated algorithm is used instead of a bundle transport algorithm;
- sub-grid temperature integrations are significantly optimized by physical and mathematical simplifications associated with the k -distribution spectral formulation (exponential extinction and bypassing of spectral correlation difficulties [13–18]).

Section 2 begins on a monochromatic basis with simple one-dimensional geometries, discussing spatial integration procedures. Generalization is then made to any geometries. At this stage a net-exchange re-formulation is further introduced and convergence illustrations are made on the basis of simple one-dimensional slab configurations.

Section 3 introduces the k -distributions Monte Carlo spectral integration approach, discussing sampling probability choices. The same test case is used for convergence illustrations considering narrow-band integrated radiative powers, on the basis of Malkmus model [10], for a wide range of line overlap parameters and average optical thicknesses.

2. Optics and geometries

Using k -distribution approaches for spectral integration allows one to consider all optic and geometric integrations on a pseudo-monochromatic basis (see Section 3). Transmission functions are therefore exponential functions, which in the frame of MC integration allows simple variance reduction techniques to be implemented, in particular as far as sub-grid integration is concerned. For the sake of clarity, in the present section, optic and geometry are discussed assuming a non-scattering, uniformly absorbing medium. Both assumptions may be easily relaxed as in any standard Monte Carlo algorithm.²

2.1. Sub-grid integration

In order to illustrate the behavior of standard MC algorithms as function of optical thickness and to introduce the principle of the proposed algorithm, the simple problem of monochromatic slab emission is first analysed. This permits the derivation of analytical solutions and associated variances from which our choices of optimized probability density functions may be physically discussed and tested.

Consider a horizontal slab of semi-transparent medium between black boundaries. The slab thickness is L and the downward unit vector normal to the slab is written \vec{n} (see Fig. 1). The temperature

² Scattering is usually represented via random generation of scattering positions and angles, the MC algorithm being kept unchanged on the basis of broken lines optical paths instead of straight lines [2]. Non-homogeneous absorption creates no source of difficulty provided that the variations of absorption coefficient are known along each optical path, which in the frame of the k -distribution approach may be achieved using the correlated- k assumption [13,17].

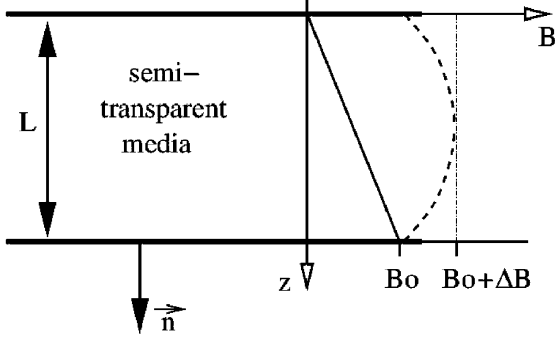


Fig. 1. Non isothermal 1D slab configuration —: linear blackbody intensity profile; - - - parabolic blackbody intensity profile.

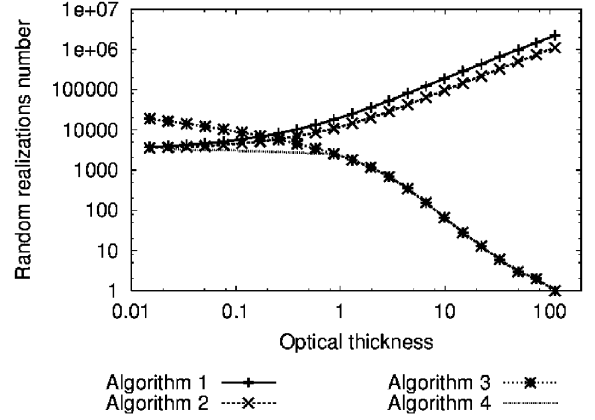


Fig. 2. Number of required bundle realizations for MC estimation of inhomogeneous slab emission with a 1% relative error, as function of slab optical thickness. Results corresponding to Algorithms 1, 2 and 3 are analytical, whereas the results of Algorithm 4 were obtained with effective MC simulations.

profile is such that the monochromatic blackbody intensity at the considered frequency follows a linear profile from B_0 at the bottom to 0 at the top.

Downward radiative flux at the bottom can be expressed as

$$\begin{aligned}
 F &= \int_{2\pi} d\omega(\vec{u}) \int_0^L dz k \exp\left(-\frac{kz}{\vec{u} \cdot \vec{n}}\right) B_0(1 - z/L) \\
 &= 2\pi B_0 \left(1/2 - \frac{1}{3kL} + \frac{E_4(kL)}{kL}\right),
 \end{aligned} \tag{1}$$

where E_n is the n th exponential integral.

Algorithm 1. In the most straightforward MC algorithm, sampling events are randomly generated in a way that preserves a close analogy with photon transport statistics. As far as the present test case is concerned, z and \vec{u} are sampled according to respectively uniform and isotropic probability density functions. F is then estimated counting bundles reaching the bottom boundary before absorption, which may be formally represented via the following expression:

$$F = \int_0^L dz p_Z(z) \int_{2\pi} d\omega(\vec{u}) p_\Omega(\vec{u}) \int_0^{+\infty} d\sigma p_\Sigma(\sigma) w_1(z, \vec{u}, \sigma) \tag{2}$$

with

$$w_1(z, \vec{u}, \sigma) = 2kL\pi B_0(1 - z/L) \mathcal{S}\left(\sigma - \frac{z}{\vec{u} \cdot \vec{n}}\right),$$

where \mathcal{S} is a step function: $\mathcal{S}(a) = 0$ if $a < 0$ and $\mathcal{S}(a) = 1$ otherwise. The position of emission in the one-dimensional slab is produced by generating randomly the abscissa z according to $p_Z(z) = 1/L$. The direction of emission is generated according to $p_\Omega(\vec{u}) = 1/2\pi$. Then z and \vec{u} define a line of sight along which a virtual absorption position is generated according to an exponential pdf between 0

and $+\infty$: $p_\Sigma(\sigma) = k \exp(-k\sigma)$. This leads to a bundle weight $w^1 = w_1^*(z) = 2kL\pi B_0(1 - z/L)$ when the bundle reaches the bottom boundary, $w_1 = 0$ otherwise. The radiative flux addressed corresponds to the average weight: $F = \langle w_1 \rangle$. The practical algorithm uses a finite number N of emission-absorption events to estimate F as the average of corresponding weights and such an estimate is associated with a statistical error

$$\mathcal{E}_{v,1} = \sqrt{\frac{1}{N}(\langle w_1^2 \rangle - \langle w_1 \rangle^2)}. \quad (3)$$

In the present simple case, this error can be obtained analytically as

$$\mathcal{E}_{v,1} = \frac{2\pi B_0}{\sqrt{N}} \sqrt{\frac{kL}{2} - \frac{2}{kL} E_5(kL) - \frac{2}{3} + \frac{1}{4kL} - \left(\frac{F}{2\pi B_0}\right)^2}.$$

The ‘‘pathological’’ behavior of such MC algorithms for strong optical thicknesses can be seen noticing that $\mathcal{E}_{v,1}/F \simeq \sqrt{2kL/N}$ when $kL \gg 1$ and therefore that the relative error tends to infinity when optical thickness tends to infinity. Fig. 2 displays the number of random generations required for a 1% relative error as a function of optical thickness. In terms of physical images, this behavior can be explained by the fact that for strong optical thicknesses, most bundles are absorbed within the slab; therefore only a few bundles contribute to the radiative flux at the boundary and the statistics require large numbers of emitted bundles for satisfactory accuracies.

Algorithm 2. This interpretation could lead one to believe that path integrated MC algorithms, in which all bundles leave the emitting volume element (no complete self absorption), would have better statistical behaviors. In these algorithms, bundles are emitted as described above with the same initial weight $w_2^*(z) = w_1^*(z)$, but instead of being absorbed at one single absorption position, each bundle undergoes an exponential attenuation along the defined ray until the bottom boundary is encountered. In our case, such an algorithm corresponds to the following formulation:

$$F = \int_0^L dz p_Z(z) \int_{2\pi} d\omega(\vec{u}) p_\Omega(\vec{u}) w_2(z, \vec{u}) \quad (4)$$

with

$$w_2(z, \vec{u}) = 2kL\pi B_0(1 - z/L) \exp\left(-\frac{kz}{\vec{u} \cdot \vec{n}}\right).$$

Events are defined with only two random generations (emission position and direction, no absorption position). As before, $F = \langle w_2 \rangle$ and for a practical MC calculation with N events, the statistical error is

$$\mathcal{E}_{v,2} = \frac{2\pi B_0}{\sqrt{N}} \sqrt{\frac{kL}{4} - \frac{1}{4kL} E_5(2kL) - \frac{1}{6} + \frac{1}{16kL} - \left(\frac{F}{2\pi B_0}\right)^2}.$$

For strong optical thicknesses, this relative error simplifies to $\mathcal{E}_{v,2}/F \simeq \sqrt{kL/N}$, which is better than that of a straightforward bundle transport algorithm but still tends to infinity with increasing optical thicknesses. Path integrated algorithms therefore encounter equivalent bad behaviors. The reason is

that, although complete auto-absorptions have been suppressed, only bundles emitted in the immediate vicinity of the boundary leave the volume with a significant weight; all other bundles are strongly attenuated and reach the boundary with a quasi-zero weight. The statistical difficulties are therefore very similar. The number of bundles required for a one percent relative error with Algorithm 2 are displayed in Fig. 2 and can be compared with that of Algorithm 1.

Algorithm 3. In both the above cases, the difficulties are obviously associated with emission position random generations. These difficulties can be relieved by modification of $p_Z(z)$ to choose emission positions close to the boundaries. However, exponential extinction depends on emission angles and radiation may come from further inside the slab for quasi-normal directions whereas only the very bottom of the slab contributes to quasi-tangential fluxes. It appears therefore that angular and spatial integrals ought to be inverted and emission directions generated before emission positions. If the direction \vec{u} is generated first, an adapted pdf of z knowing \vec{u} can be chosen to match exactly the exponential attenuation from z to the boundary. This adapted pdf is:

$$p_{Z,a}(z; \vec{u}) = \frac{\frac{k}{\vec{u} \cdot \vec{n}} \exp\left(-\frac{kz}{\vec{u} \cdot \vec{n}}\right)}{1 - \exp\left(-\frac{kL}{\vec{u} \cdot \vec{n}}\right)}. \quad (5)$$

As for all biased MC algorithms, the bundle weight must be adjusted in accordance with the new pdf choice, which implies here that the previous bundle weight $w_2^*(z)$ should be replaced by

$$\frac{1 - \exp\left(-\frac{kL}{\vec{u} \cdot \vec{n}}\right)}{\exp\left(-\frac{kz}{\vec{u} \cdot \vec{n}}\right)} 2\pi(\vec{u} \cdot \vec{n})B_0(1 - z/L).$$

The fact that $\vec{u} \cdot \vec{n}$ appears as product in this bundle weight expression would introduce an undesired distribution width in the optically thick limit. As a first step, to illustrate that MC algorithms may be simply adapted to deal with optically thick configurations, this difficulty can be bypassed via a modification of the angular distribution using $p_{\Omega,l}(\vec{u}; \vec{n}) = \vec{u} \cdot \vec{n}/\pi$. The initial bundle weight then becomes

$$w_3^*(z) = \frac{1 - \exp\left(-\frac{kL}{\vec{u} \cdot \vec{n}}\right)}{\exp\left(-\frac{kz}{\vec{u} \cdot \vec{n}}\right)} \pi B_0(1 - z/L).$$

Altogether, the corresponding optimized algorithm consists of the following: (i) directions are generated randomly according to $p_{\Omega,l}(\vec{u}; \vec{n})$ which corresponds to a Lambert angular distribution; (ii) positions are allotted randomly according to the exponential distribution $p_{Z,a}(z; \vec{u})$; (iii) bundles are allotted the initial weight $w_3^*(z)$; (iv) the rest of the algorithm is kept unchanged, either a bundle transport or a path integrated algorithm. Applying this algorithm in its ray-tracing form to the same test case as above corresponds formally to the following expression:

$$F = \int_{2\pi} d\omega(\vec{u}) p_{\Omega,l}(\vec{u}; \vec{n}) \int_0^L dz p_{Z,a}(z; \vec{u}) w_3(z, \vec{u}) \quad (6)$$

with

$$w_3(z, \vec{u}) = \left[1 - \exp\left(-\frac{kL}{\vec{u} \cdot \vec{n}}\right) \right] \pi B_0 (1 - z/L)$$

and the corresponding statistical error is

$$\mathcal{E}_3 = \frac{2\pi B_0}{\sqrt{N}} \sqrt{\frac{1}{4} - \frac{1}{3kL} + \frac{1}{4(kL)^2} - \frac{2E_5(kL)}{k^2 L^2} - \frac{E_3(kL)}{2} - \frac{1}{kL} E_4(kL) + \frac{E_5(2kL)}{k^2 L^2} - \left(\frac{F}{2\pi B_0}\right)^2}.$$

Unlike the other two algorithms, the relative error does not tend to infinity with increasing optical thickness, but instead decreases to zero as $\mathcal{E}_3/F \simeq (1/3kL)\sqrt{5/N}$. Fig. 2 displays the numbers of bundles required to reach a 1% relative error and illustrates that the adapted algorithm encounters no specific difficulty for strong optical thicknesses.

Algorithm 4. This last Algorithm 3 shows however worse behavior than the two preceding in the optically thin limit. Such behavior is due to angular integration: the Lambert distribution ($p_{\Omega,l}(\vec{u}; \vec{n}) = \vec{u} \cdot \vec{n}/\pi$) is indeed adapted to optically thick system emissions but not to thin ones that tend to isotropy ($p_{\Omega}(\vec{u}) = 1/2\pi$). This dependence on optical thickness may for instance be approached using an angular pdf that combines both limit cases:

- The Lambert law is kept for systems with optical thickness greater than unity:

$$p_{\Omega,a}(\vec{u}; \vec{n}, kL) = p_{\Omega,l}(\vec{u}) \quad \text{if } kL > 1$$

- For systems with optical thickness lower than unity, a Lambert like distribution is used for slab tangential directions and a uniform distribution for close to normal directions:

$$p_{\Omega,a}(\vec{u}; \vec{n}, kL) = \frac{1}{1 - kL/2} \left(\mathcal{S}(kL - \vec{u} \cdot \vec{n}) \frac{1}{2kL} \frac{\vec{u} \cdot \vec{n}}{\pi} + \mathcal{S}(\vec{u} \cdot \vec{n} - kL) \frac{1}{2\pi} \right). \quad (7)$$

The algorithm then formally corresponds to

$$F = \int_{2\pi} d\omega(\vec{u}) p_{\Omega,a}(\vec{u}; \vec{n}, kL) \int_0^L dz p_{Z,a}(z; \vec{u}) w_4(z, \vec{u}) \quad (8)$$

with

$$w_4(z, \vec{u}) = w_3(z, \vec{u}) \frac{p_{\Omega,l}(\vec{u}; \vec{n})}{p_{\Omega,a}(\vec{u}; \vec{n}, kL)}.$$

Numerical results obtained with Algorithm 4 are reported in Fig. 2 showing good behavior in both optically thin and optically thick limits.

2.2. Generalized algorithmic procedure

The preceding simple example (Monte Carlo estimation of the power emitted from a non-isothermal slab to a surface) illustrated how important it is to work on both the formulation choice and the

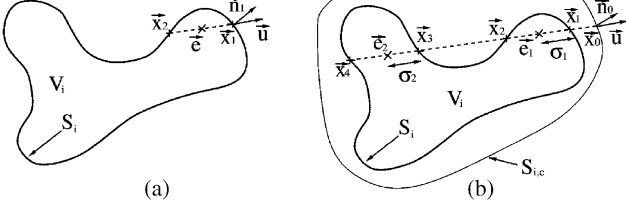


Fig. 3. Emission positions and emission directions. (a) Integration over the envelope. (b) Integration over a convex surrounding surface (see Appendix A).

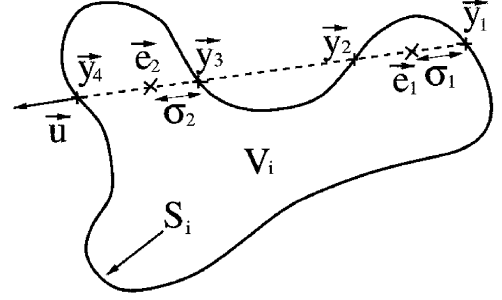


Fig. 4. Absorption segments and exchange positions.

pdf adaptations to deal with optically thick conditions. A general three-dimensional Monte Carlo algorithm is presented hereafter that benefits from these observations concerning sub-grid integration optimization, generalizing the principle of Algorithm 4 to any geometry. For the sake of clarity, the algorithm is formally enunciated assuming black system boundaries, and the required extension associated with surface reflexions are rapidly treated via independent footnotes.

Let us consider a system divided into N_V volume elements V_i of semi-transparent material and N_S opaque surface elements S_i . Volume and surface elements are non-isothermal and the volume elements cannot be assumed optically thin. The temperature field will be described as a continuous field and the corresponding blackbody intensity field at the considered frequency will be noted $B(\vec{x})$ where \vec{x} is the coordinate vector.

When computing exchange rates from a volume to a surface, $\varphi(V_i, S_j)$ (the radiative power emitted by V_i that is absorbed by S_j), or between two volume elements, $\varphi(V_i, V_j)$, with bundles starting from V_i , the first step is the random generation of an emission position \vec{e} within V_i and of an emission direction \vec{u} . The most direct extension of Algorithm 4 to three-dimensional geometries consists in the following procedure (see Appendix and Fig. 3a):

- (1) A position \vec{x}_1 is uniformly and randomly generated on V_i 's envelope, noted³ \mathcal{S}_i : $p_S(\vec{x}_1) = 1/\mathcal{S}_i$.
- (2) The emission direction \vec{u} is randomly generated on the outward hemisphere at \vec{x}_1 according to the previously defined pdf adapted as function of V_i 's optical thickness: $p_\Omega(\vec{u}; \vec{n}_1, kL)$ (see Eq. (7)) where \vec{n}_1 is the outward oriented unit vector normal to \mathcal{S}_i at \vec{x}_1 . In the one dimensional case the length L was chosen as the slab thickness, but in the general case L should be taken as a length scale characteristic of V_i 's thickness from \vec{x}_1 's view point.
- (3) \vec{x}_1 and \vec{u} are used to define a continuous segment within V_i from \vec{x}_1 to \vec{x}_2 , where \vec{x}_2 is the first intersection with \mathcal{S}_i starting from \vec{x}_1 in the direction $-\vec{u}$.
- (4) The emission position \vec{e} is randomly generated along the segment $[\vec{x}_1, \vec{x}_2]$ according to an exponential distribution:

$$\vec{e} = \vec{x}_1 - \sigma \vec{u} \quad \text{with} \quad p_\Sigma(\sigma) = \frac{k \exp(-k\sigma)}{1 - \exp(-k\|\vec{x}_2 - \vec{x}_1\|)}.$$

³ Depending on the geometries, generating \vec{x}_1 on the envelope \mathcal{S}_i may be tedious, in which case the alternative procedure described in Appendix may be preferred.

At this stage, emission position and direction have been randomly generated to define a line of sight leaving V_i at \vec{x}_1 . A bundle is then followed along this direction starting at \vec{x}_1 with the following initial bundle weight:

$$w_0^* = \pi \mathcal{S}_i [1 - \exp(-k \|\vec{x}_2 - \vec{x}_1\|)] \frac{p_{\Omega,l}(\vec{u}; \vec{n}_1)}{p_{\Omega,a}(\vec{u}; \vec{n}_1, kL)}. \quad (9)$$

As in any ray-tracing algorithm, the bundle weight is exponentially attenuated along its path as a function of the amount of encountered absorber. At any location \vec{y} , the remaining bundle weight is noted $w^*(\vec{y})$ and satisfies $w^*(\vec{y}) < w_0^*$.

When computing $\varphi(V_i, S_j)$ with N such emission events, each bundle is followed until S_j is encountered at location \vec{a} . The Monte Carlo weight is then computed as

$$w(\vec{e}, \vec{a}) = w^*(\vec{a})B(\vec{e}) \quad (10)$$

and $\varphi(V_i, S_j)$ is estimated as the average weight $\langle w \rangle_N$. For optical paths where complete absorption occurs before S_j is encountered, the event is attributed a weight⁴ $w = 0$.

Generally speaking, the line of sight intersects any volume element V_j in m segments $[\vec{y}_{2l-1}, \vec{y}_{2l}]$ with $l=1, \dots, m$ (see Fig. 4). When computing $\varphi(V_i, V_j)$, the ray is therefore followed until complete absorption, defining these m segments and the Monte Carlo weight is computed as

$$w(\vec{e}, \vec{y}_1, \dots, \vec{y}_{2m}) = \sum_{l=1}^m w^*(\vec{y}_{2l-1}) [1 - \exp(-k \|\vec{y}_{2l} - \vec{y}_{2l-1}\|)] B(\vec{e}). \quad (11)$$

When computing $\varphi(S_i, S_j)$ and $\varphi(S_i, V_j)$ starting from S_i , the algorithm is strictly similar in the limit case of $L = +\infty$: emission positions are generated uniformly on S_i ($\sigma = 0$); the angular distribution becomes Lambert distribution ($p_{\Omega,a}(\vec{u}; \vec{n}_1, +\infty) = p_{\Omega,l}(\vec{u}; \vec{n}_1)$); and the initial weight becomes⁵ $w_0^* = \pi S_i$. The proposed algorithm allows therefore a continuous treatment of sub-system emissions, from optically thin volumes to opaque surfaces, via optimized pdf choices for the total range of system optical thicknesses.

At this stage the algorithm is a forward algorithm in the sense that quantities addressed are exchange rates from one geometrical element to another. As discussed in the introduction section, net-exchange algorithms have been shown to ensure better convergence in numerous configurations.

⁴ When simulating black boundary cavities, complete absorption occurs at the first boundary encounter and S_j may only be encountered once. In the case of reflecting boundaries, the optical path is continued after each surface encounter generating randomly a reflexion direction according to the local directional-directional reflectivity function. At each such reflexion, the weight is attenuated according to the directional absorptivity ($w^* \rightarrow (1 - \alpha)w^*$) and the path is interrupted when $w^* < \varepsilon/\Delta B_{\max}$ is satisfied, where ε is the required accuracy and ΔB_{\max} the maximum absolute blackbody intensity difference between the emission point and any other location in the cavity. Such a multiple broken line optical path may encounter S_j at several locations $\vec{a}_1, \dots, \vec{a}_m$ under incident directions corresponding to directional absorptivities $\alpha_1, \dots, \alpha_m$ and the MC weight is computed as

$$w(\vec{e}, \vec{a}_1, \dots, \vec{a}_m) = \sum_{l=1}^m \alpha_l w^*(\vec{a}_l) B(\vec{e}).$$

⁵ In case of a non-black surface, w_0^* is multiplied by the directional emissivity.

For the sake of numerical quality, it is therefore preferable to further add this net-exchange reformulation step to the preceding algorithm which may be very simply performed thanks to the reciprocity principle. One may refer to [6,19] and [20] for details concerning net-exchange formulations, but the essential picture is that quantities addressed are net-exchange rates between geometrical elements. The net-exchange rate $\psi(V_i, V_j)$ between volumes V_i and V_j is the power emitted by V_i and absorbed by V_j minus the power emitted by V_j and absorbed by V_i :

$$(V_i, V_j) = \varphi(V_i, V_j) - \varphi(V_j, V_i).$$

The radiative balance of any element is therefore the sum of all net-exchange rates with other discretization elements. Independently of the physical insight that net-exchange formulations may provide to radiative transfer problems, numerical benefit associated with this formulation is that it intrinsically satisfies the reciprocity principle. Apart from configurations in which strongly irregular discretizations are required, one may think of configurations in which dominant radiative exchanges occur between elements at similar temperature levels. The reason why in such cases net-exchange formulations lead to better numerical behavior than standard forward formulations is simply that when two elements are at similar temperature levels the two reciprocal exchange rates are numerically close to each other. The difference between these two exchange rates, that is the contribution to the radiative balance, may therefore be very small compared to exchange rates themselves. A numerical estimation procedure based on independent exchange rates estimations may therefore lead to very high levels of uncertainties (difference of two approximate quantities of similar magnitudes). In numerical methods based on net-exchange formulations, the quantities addressed are directly the net-exchange rates between elements and this difference taking step is bypassed.

This is particularly relevant to optically thick configurations in which main radiative exchanges occur between adjacent elements and correspond to exchange locations that are very close to the interface. These locations are therefore likely to correspond to very similar temperature levels.

As shown in [19] our forward Monte Carlo algorithm may be turned into a net-exchange algorithm via an additional step of absorption location random generation within each absorption segment. In practice, this means that the algorithm is kept strictly identical to what was presented above except that each time an absorption segment $[\vec{y}_{2l-1}, \vec{y}_{2l}]$ is identified. An absorption position \vec{a}_l is randomly generated (as for emission) according to an exponential distribution:

$$\vec{a}_l = \vec{y}_{2l-1} + \sigma \vec{u} \quad \text{with} \quad p_\Sigma(\sigma) = \frac{k \exp(-k\sigma)}{1 - \exp(-k\|\vec{y}_{2l} - \vec{y}_{2l-1}\|)}.$$

Monte Carlo weights are then modified by replacing blackbody intensities at the emission position $B(\vec{e})$ by blackbody intensity differences between emission and absorption positions. Eqs. (10) and (11) therefore simply become

$$w(\vec{e}, \vec{a}) = w^*(\vec{a})[B(\vec{e}) - B(\vec{a})] \tag{12}$$

for interaction with a surface and

$$w(\vec{e}, \vec{y}_1, \dots, \vec{y}_{2m}, \vec{a}_1, \dots, \vec{a}_m) = \sum_{l=1}^m w^*(\vec{y}_{2l-1})[1 - \exp(-k\|\vec{y}_{2l} - \vec{y}_{2l-1}\|)][B(\vec{e}) - B(\vec{a}_l)] \tag{13}$$

for interaction with a volume. The average values of these new Monte Carlo weights are now estimated from N realizations to approximate the net exchange rates $\psi(V_i, S_j)$ and $\psi(V_i, V_j)$ directly.

2.3. Convergence illustration (monochromatic)

Simple configurations (one dimension slab) are used for convergence quality illustration. Simulations are first performed on a monochromatic basis and similar examples are later reconsidered in Section 3 with an additional integration over gaseous line spectra.

The slab geometry is that of Fig. 1. The boundaries are black and absorption coefficient is uniform. The first test case is that proposed in [5] for comparison of forward bundle transport algorithm, forward path integrated algorithm and reverse path integrated algorithm.⁶ The temperature profile is such that the monochromatic blackbody intensity at the considered frequency is B_0 at the boundaries and uniform at $B_0 + \Delta B$ across the slab. Estimated quantities are radiative flux divergence averages within each of the 10 regular layers used for slab discretization.

For slab optical thickness $kL=10$, Fig. 5 presents successively the exact and Monte Carlo solutions, the percent error presented in [5] for the three tested strategies (in the specific case of $B_0=0$) and the percent error reached with our proposed adapted net-exchange methodology (which is independent of B_0 owing to the net-exchange formulation). All corresponding simulations are performed using 10,000 ray sampling per element. The conclusion of this first exercise is undoubtedly the same as that of Fig. 2: a simple reformulation of the emission position and emission angle integrals allows one to solve the well known problem of Monte Carlo convergence for optically thick configurations. To further illustrate this point, Fig. 6 displays the radiative flux divergence averages (and statistical error) within layer 1 (against the boundary) and layer 5 (one of the two central layers) as a function of optical thickness widely above $kL = 10$. These simulations confirm that in the proposed scheme statistical errors are insensitive to optical thickness in the optically thick limit.

However, this first test case is not very representative of practical optically thick configurations in which most of the physics lies in the energy redistribution process within the medium via short distance photon exchanges. Treatment of non-uniform temperature profiles is essential keeping in mind the limiting case of the Rosseland approximation in which energy transfers are modeled on the basis of second order spatial derivatives (as for any diffusion process). In our second test case, the temperature profile is therefore chosen such that the monochromatic blackbody intensity at the considered frequency follows a parabolic profile across the slab, from B_0 at the boundary to $B_0 + \Delta B$ at the slab center. Slab discretization is now performed on the basis of 20 layers of equal width. Fig. 7 displays simulation results and statistical errors for three optical thicknesses ($kL = 0.1$, $kL = 1$ and $kL = 10$) for 10,000 ray samplings per element. Similarly, Fig. 8 displays the results obtained for layer 3 and layer 10 as a function of optical thickness.

Statistical errors are necessarily higher for this second test case than for the isothermal slab: sub-grid temperature profile integration is now essential whereas only the angular integration had to be statistically reconstructed in preceding test case. Worth some attention is the fact that errors are higher close to the boundaries than at the center of the slab. After a close look at this behavioral difference, it appears that this is not a boundary effect. It is related to the temperature profile only:

⁶ The corresponding denominations used in [5] are the forward collision based algorithm, forward pathlength algorithm and reverse algorithm respectively.

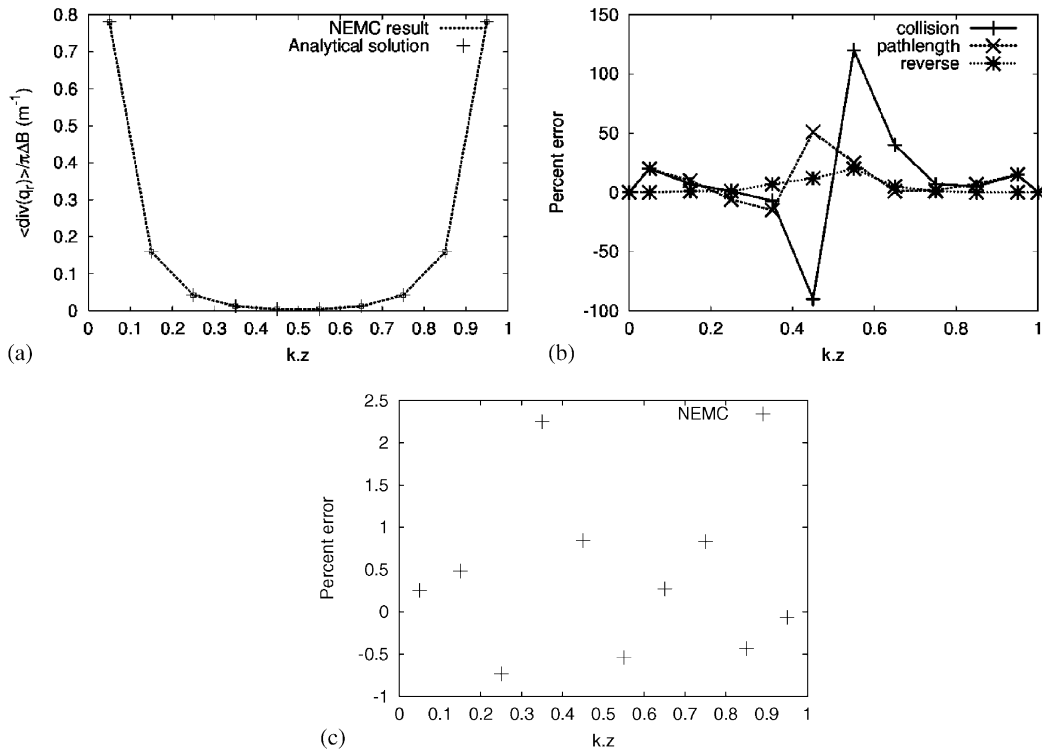


Fig. 5. Comparison of the proposed net-exchange Monte-Carlo (NEMC) approach against “collision based”, “pathlength” and “reverse” algorithms as reported in [5]. The computations are on a monochromatic basis. The test case is a uniform one-dimensional slab at $B_0 + \Delta B$ with black boundaries at B_0 discretized in 10 regular layers. Presented quantities are radiative flux divergence averages for each layer normalized by $\pi \Delta B$. 10,000 sampling events per discretization element are used for each algorithm. In [5] computations were performed with $B_0 = 0$ whereas NEMC behaviors are insensitive to B_0 . (a) Analytical and NEMC solutions. (b) Percent errors as reported in [5]. (c) Percent errors as obtained with NEMC.

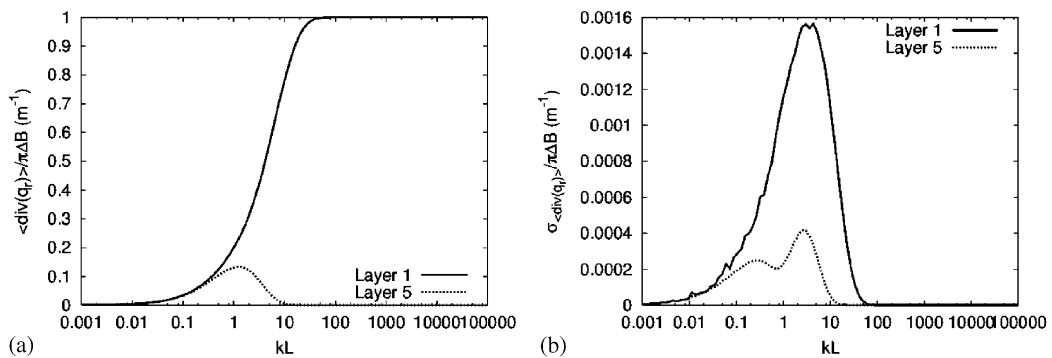


Fig. 6. (a) Radiative flux divergence averages for layer 1 (against the boundary) and layer 5 (at slab center) as functions of slab optical thickness for the same test case as in Fig. 5. (b) Corresponding MC standard deviation (statistical errors).

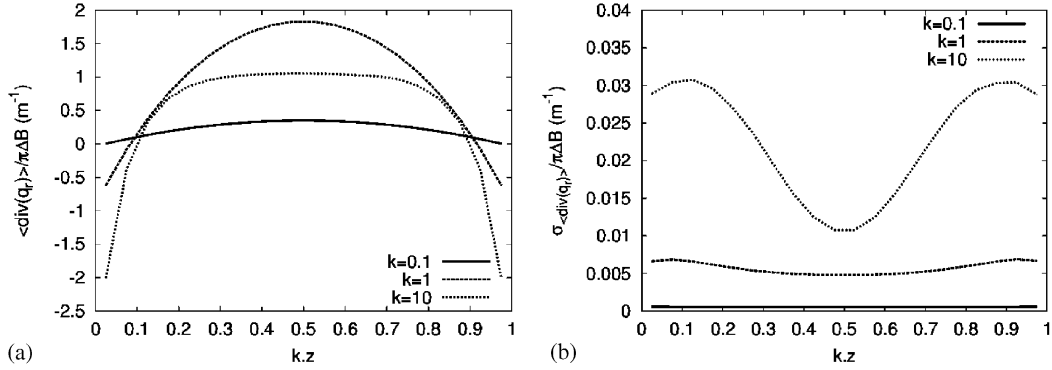


Fig. 7. (a) Estimated radiative flux divergence averages, using the proposed net-exchange Monte-Carlo approach using 10,000 sampling events per discretization element. The test case is a 1D slab with black boundaries. Computations are held on a monochromatic basis. Absorption coefficient is uniform. The blackbody intensity profile is parabolic from B_0 at the boundaries to $B_0 + \Delta B$ at the center. The slab is discretized in 20 regular layers. (b) Corresponding MC standard deviation (statistical errors).

this profile is such that the second order spatial derivative of the monochromatic blackbody intensity is constant (which explains why the radiative flux divergence tends to a flat profile when increasing optical thickness), but the net energy transfer rate of each layer is being computed essentially as the sum of two net-exchange rates with neighboring layers. Numerical conditions are very distinct for layer 3 and layer 10 for instance. For layer 3, blackbody intensity gradients are of similar magnitude at both interfaces and the net energy transfer rate is therefore computed as the difference of two uncertain net-exchange rates of similar magnitudes. Statistical errors on radiative net-exchanges are therefore amplified by this difference taking step. This difficulty is not encountered with layer 10 because the parabolic profile is flat at the slab center which means that the net-exchange rate between layer 10 and layer 11 tends to zero with increasing absorption. Reducing this sensitivity of the algorithm to the sub-grid temperature profile could be partly achieved via an explicit representation of this spatial dependence in the pdf choice for emission position sampling. But at the present stage, without a specific high accuracy requirement, the results seem quite acceptable (never more than a few percent error with 10,000 ray samplings), especially when thinking of complete divergences as are commonly encountered with standard Monte Carlo algorithms in the optically thick limit.

3. Spectral integration

3.1. Principles

In the preceding section, MC integrations were considered on a monochromatic basis, optimizing the algorithm in such a way that satisfactory convergence is ensured for all types of optical thicknesses. The motivation for this optimization attempt was that when considering spectral integration over line spectra, a large range of optical thicknesses may be encountered from very high thicknesses at line centers to optically thin configurations between lines.

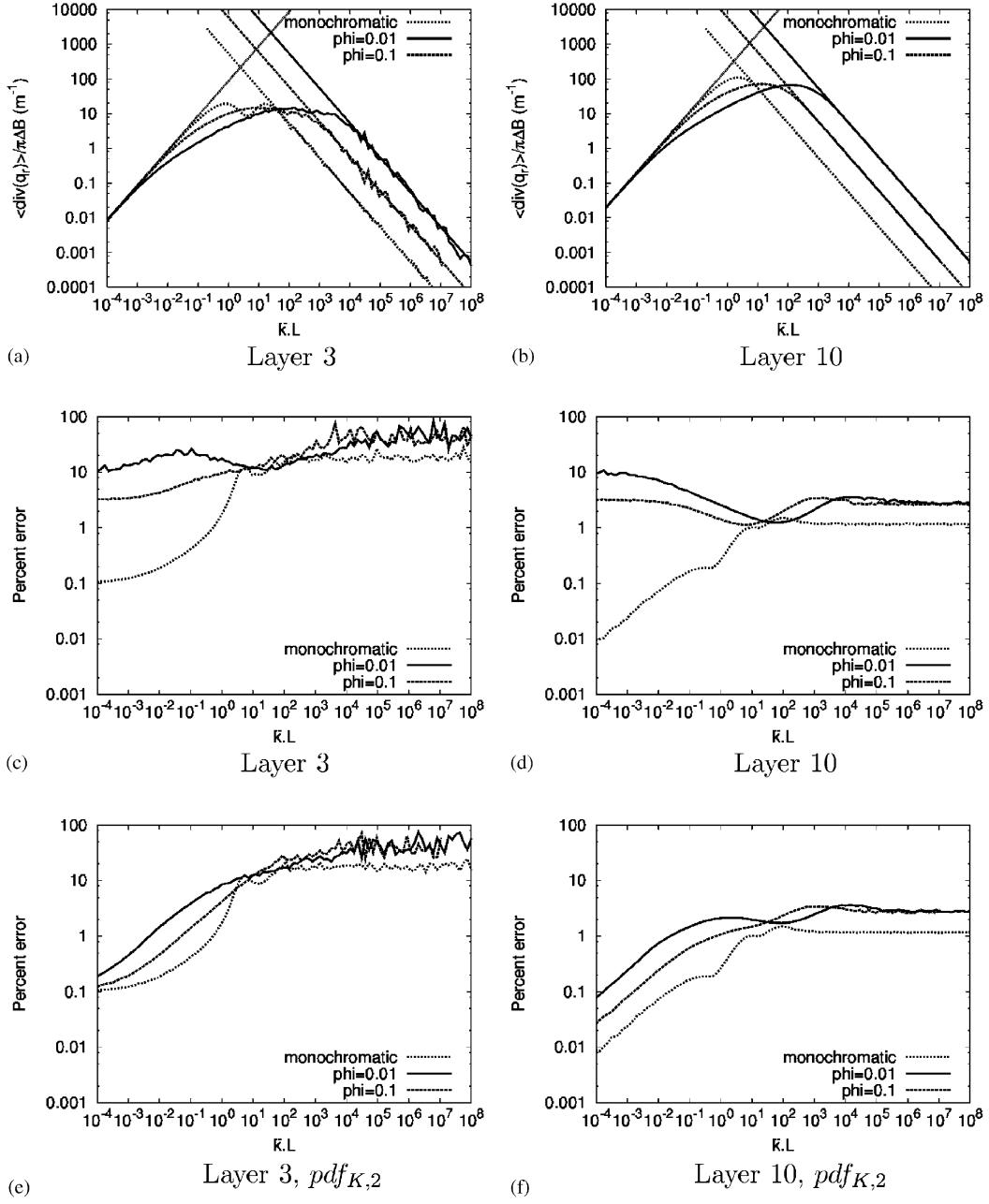


Fig. 8. Radiative flux divergence averages (a and b) and standard deviations (statistical errors, c, d, e and f) for layer 3 and layer 10 as a function of slab optical thickness for the same test case as in Fig. 7. Also presented are computations performed on a narrow band interval using Malkmus model as a function of average optical thickness $\bar{k}L$ for two values of the shape parameter (line overlap parameter): $\Phi = 0.1$ and $\Phi = 0.01$. Analytical solutions corresponding to the optically thin and optically thick models are presented as straight lines for comparison. Standard deviations in c and d correspond to the use of $pdf_{K,1}(k) = f(k)$ for k -sampling, whereas e and f correspond to the use of $pdf_{K,2}(k)$, see Eq. (21).

When computing integrated exchange (or net-exchange) rates over a spectral interval $[v_{\min}, v_{\max}]$ with a MC algorithm, the only step to be added to the preceding algorithms is the random generation of a frequency v within $[v_{\min}, v_{\max}]$ according to an arbitrarily chosen pdf. As for optic and geometric considerations, this pdf is essential in the sense that numerical convergence depends on its choice. In order to formalise this point, let us write the spectrally integrated net-exchange rate between volumes V_i and V_j using a synthetic path-integral formulation in which $\Gamma_v(V_i, V_j)$ is the space of all possible optical paths γ , at frequency v , and $h_\psi(\gamma, v)$ is the contribution of monochromatic net exchange along Γ :

$$(V_i, V_j) = \int_{v_{\min}}^{v_{\max}} dv \psi_v(V_i, V_j) = \int_{v_{\min}}^{v_{\max}} dv \int_{\Gamma_v(V_i, V_j)} d\gamma h_\psi(\gamma, v). \quad (14)$$

As before, pdf's are introduced for integration variables v and γ and Monte Carlo estimates are obtained on the basis of corresponding sampling events:

$$\begin{aligned} (V_i, V_j) &= \int_{v_{\min}}^{v_{\max}} dv pdf_N(v) \int_{\Gamma_v(V_i, V_j)} d\gamma pdf_\Gamma(\gamma) w_\psi(\gamma, v) \\ &\approx \frac{1}{N} \sum_{n=1}^N w_\psi(\gamma_n, v_n), \end{aligned} \quad (15)$$

where γ_n and v_n are N random generations of optical path and frequency according to pdf_Γ and pdf_N , and where the MC weight w_ψ is computed as

$$w_\psi(\gamma, v) = \frac{h_\psi(\gamma, v)}{pdf_N(v) pdf_\Gamma(\gamma)}.$$

For a given frequency, optimizing optical path sampling was the object of Section 2: $pdf_\Gamma(\gamma)$ is therefore nothing but a formal representation of spatial and angular sampling procedures that were carefully discussed above as a function of optical thickness. The remaining question is therefore that of optimizing the frequency pdf choice. In this optimization exercise, the variance of $w_\psi(\gamma_n, v_n)$ must be as low as possible, keeping $pdf_N(v)$ simple enough to handle for practical random sampling. This compromise is extremely difficult to reach when dealing with gaseous infrared spectra such as those of water vapor and carbon dioxide. The spectral variations of the radiative transfer functions to be integrated are so sharp and irregular that it seems not feasible to design sufficiently simple spectral pdf's that could compensate for h_ψ 's variations.

Very strong simplifications may however be introduced when the spectral interval is narrow enough for blackbody intensities, surface reflexion properties and scattering properties to be assumed independent of frequency: this is the narrow band assumption that is a common basis for all so-called narrow band spectral integration models. Under this assumption, the function to be integrated depends only on frequency through the spectral dependence of absorption coefficients, which offers the opportunity for narrow band k -distribution methodology to be applied:

- A new function \tilde{h} is introduced that explicitly defines the absorption coefficient dependence:
 $h_\psi(\gamma, v) = \tilde{h}_\psi(\gamma, k_v).$

- The distribution of absorption coefficients within the interval $[v_{\min}, v_{\max}]$ is noted $f(k)$ (the inverse transmission function [11]) and is modeled to the level of required accuracy.
- (V_i, V_j) may then be re-written in a way that justifies a new MC algorithm in which random absorption coefficients are generated instead of random frequencies:

$$\begin{aligned}
(V_i, V_j) &= [v_{\max} - v_{\min}] \int_{k_{\min}}^{k_{\max}} dk f(k) \int_{\Gamma(V_i, V_j)} d\gamma \tilde{h}_{\psi}(\gamma, k) \\
&= \int_{k_{\min}}^{k_{\max}} dk pdf_K(k) \int_{\Gamma(V_i, V_j)} d\gamma pdf_{\Gamma}(\gamma) \tilde{w}_{\psi}(\gamma, k) \\
&\approx \frac{1}{N} \sum_{n=1}^N \tilde{w}_{\psi}(\gamma_n, k_n)
\end{aligned} \tag{16}$$

with

$$\tilde{w}_{\psi}(\gamma, k) = [v_{\max} - v_{\min}] \frac{f(k)}{pdf_K(k)} \frac{\tilde{h}(\gamma, k)}{pdf_{\Gamma}(\gamma)}.$$

Note that the frequency dependence of optical path domain $\Gamma(V_i, V_j)$ vanishes owing to the narrow band assumption.

The main advantage of such a formulation is that the variations of the product $\tilde{h}_{\psi}(\gamma, k)f(k)$ with k are much less erratic than those of $h_{\psi}(\gamma, v)$ with frequency, so that optimizing the choice of pdf_K becomes realistic.⁷ The task of adapting the k -sampling pdf choice to the considered configuration type was studied and illustrated in [12] and three limit cases were identified:

- For computation of net exchange rates between two black surfaces at distance l :

$$pdf_K(k) = f^{ss}(k; l) = e^{-kl} f(k) / \bar{\tau}(l). \tag{17}$$

- For computation of net exchange rates between an optically thin volume and a black surface at distance l :

$$pdf_K(k) = f^{gs}(k; l) = ke^{-kl} f(k) / \bar{\tau}'(l). \tag{18}$$

- For computation of net exchange rates between two optically thin volumes at distance l :

$$pdf_K(k) = f^{gg}(k; l) = k^2 e^{-kl} f(k) / \bar{\tau}''(l), \tag{19}$$

where $\bar{\tau}(l)$ is the average transmission function. Thanks to inverse Gaussian distribution properties, these pdf's are mathematically easy to handle, provided that the considered spectrum follows the Malkmus model [12]. In the general case, the best fitted Malkmus spectrum may be used, insuring

⁷ In this presentation two distinct pdf's of k are introduced. The first one, $f(k)$ is the physical distribution of k as it appears in the considered spectrum. The second $pdf_K(k)$ is entirely arbitrary and serves only for the MC algorithm. It is however mainly on the basis of physical considerations that pdf_K may be adequately chosen, ensuring that statistical convergence is reached with an acceptable number of random generations.

first order representation of emission/absorption spectral correlations. As illustrated later, linear combinations of such limit case pdf's may be used for intermediate cases, but nevertheless the design of adapted k -sampling pdf's for each new configuration family remains a key step of such MC simulation efforts to insure fast numerical convergence.

When the spectral interval $[v_{\min}, v_{\max}]$ is not narrow enough for the narrow band assumption to be valid, the interval may be divided in N_b narrow bands of width Δv_j around v_j . Different inverse transmission functions $f_j(k)$ are introduced for each narrow band and Eq. (14) is written:

$$\begin{aligned}
(V_i, V_j) &= \sum_{b=1}^{N_b} \Delta v_b \int_{k_{\min,b}}^{k_{\max,b}} dk f_b(k) \int_{\Gamma_b(V_i, V_j)} d\gamma \tilde{h}_{\psi b}(\gamma, k) \\
&= \sum_{b=1}^{N_b} P_b \int_{k_{\min,b}}^{k_{\max,b}} dk pdf_{K,b}(k) \int_{\Gamma_b(V_i, V_j)} d\gamma pdf_{\Gamma,b}(\gamma) \tilde{w}_{\psi}(\gamma, k, b) \\
&\approx \frac{1}{N} \sum_{n=1}^N \tilde{w}_{\psi}(\gamma_n, k_n, b_n)
\end{aligned} \tag{20}$$

with

$$\tilde{w}_{\psi}(\gamma, k, b) = \frac{\Delta v_b}{P_b} \frac{f_b(k)}{pdf_{K,b}(k)} \frac{\tilde{h}_{\psi b}(\gamma, k)}{pdf_{\Gamma,b}(\gamma)}.$$

As for continuous integrals, in the frame of MC methods, discrete sums may be handled via arbitrary choices of discrete probabilities. Here N_b probabilities P_1, \dots, P_{N_b} are introduced ($\sum_{b=1}^{N_b} P_b = 1$) and narrow band index random generation are performed according to this weighting, which should be chosen to match as accurately as possible the relative contribution of each band to the final result. As discussed in [6] this unknown contribution may be estimated on the basis of simple physical reasoning, but here again the choice remains problem-dependant, and may require substantial effort for non-intuitive new configurations.

3.2. Convergence illustrations (narrow band)

This general methodology was implemented practically and tested in [21] for application to combustion configurations. We confine ourselves to academic test cases similar to those used in the preceding section in order to illustrate statistical convergence qualities as functions of average optical thickness for different types of gaseous spectra. Spectral integration is performed over a spectral band of width Δv for which the narrow band assumption is valid. The Malkmus statistical narrow band model is used so that parametric analysis is performed by varying the band average absorption coefficient \bar{k} and the shape parameter⁸ ϕ . This model is used here under its k -distribution form [11,12].

With the same 20 layer discretization as for monochromatic simulations, Fig. 8 displays radiative flux divergence averages and percent statistical errors for layer 3 and layer 10 as functions of

⁸ The shape parameter also called the line overlap parameter: $\phi = 2\gamma/\delta$ where γ is the half line width at half height and δ the average line-to-line spacing.

average optical thickness $\bar{k}L$, for two values of the shape parameter that are typical of spectrally separated gaseous spectra ($\phi = 10^{-2}$ and $\phi = 10^{-1}$). Convergence qualities associated with two distinct k -sampling pdf's are compared in terms of statistical errors for a given number of sampling events. The first one corresponds to straightforward k -sampling according to the physical distribution of absorption coefficient within the considered spectral interval: $pdf_{K,1}(k) = f(k)$ (Fig. 8c–d). The second was proposed in [21], for combustion applications, as an attempt to account for the dependence on k of pseudo-monochromatic radiative exchanges (Fig. 8e–f):

$$pdf_{K,2}(k) = \alpha_K(l)f^{gs}(k; 0) + [1 - \alpha_K(l)]f^{ss}(k; 0) \quad (21)$$

with

$$\alpha_K(l) = \frac{g^{ss}(1/l; 0) - \bar{\tau}(l)g^{ss}(1/l; l)}{1 - \bar{\tau}(l)},$$

where g^{ss} is the cumulative distribution of f^{ss} (see Eqs. (17) and (18)) and where the length l is taken as $l = L$ for surface emissions and $l = L/20$ for volume emission.

The physical reasoning leading to this adapted pdf choice is the following. In the present systems the net radiative flux at each boundary is the result of a net-exchange with a gas volume of characteristic length scale L . There is indeed no net-exchange with the opposite boundary surface because the surfaces are at the same temperature. In the case where the system may be considered optically thin, the net radiative flux at each boundary may then be seen as a net-exchange between a black surface and an adjacent optically thin gas volume; consequently, not taking into account volume temperature inhomogeneities, the best adapted k -sampling pdf is $pdf_K(k) = f^{gs}(k; 0)$. At the other extreme, where the system may be considered optically thick, always putting aside volume temperature inhomogeneities, the net radiative flux may be seen as the result of a net-exchange between two adjacent black surfaces (the boundary itself and the optically thick volume behaving like an opaque surface) and the best adapted k -sampling pdf is therefore $pdf_K(k) = f^{ss}(k; 0)$. For intermediate cases, a linear combination of both limit pdf's may be used as presented in Eq. (21). The weighting factor $\alpha_K(L)$ was chosen to reflect the fraction of the considered net-exchange due to k -values for which $kL < 1$ is satisfied:

$$\alpha_K(L) = \frac{\int_{k_{\min}}^{1/L} (1 - e^{-kL})f(k) dk}{\int_{k_{\min}}^{k_{\max}} (1 - e^{-kL})f(k) dk}$$

which leads to the above definition. When using the Malkmus model, the cumulative function g^{ss} —and therefore $\alpha_K(L)$ —take an analytical form to be found in [12].

When considering the net radiative power of a layer, a similar reasoning may be used with the physical image of a gaseous volume of characteristic length $L/20$ exchanging radiation with the rest of the gas plus the black boundaries. Again putting aside temperature inhomogeneities, there remains a simple net-exchange between a gaseous volume and an adjacent isothermal perfect absorber, which means that we return to the same optimization problem replacing system scale L with layer thickness.

The conclusion of Fig. 8 is essentially that the net-exchange procedure for integration of optics and geometrics dimensions described above, combined with the k -sampling procedure, leads to satisfactory convergence qualities for an extremely wide range of average optical thicknesses, even for spectrally marked line spectra. This is obviously directly related to the conclusions of Section 2 concerning the ability of our algorithm to deal with optically thick conditions (that are here rapidly

encountered at line center frequencies). However, it is still worth comparing Fig. 8c–d and Fig. 8e–f to illustrate how statistical convergence depends on the k -sampling pdf choice. In the optically thick limit, both the k -sampling pdf's considered are identical as $\lim_{\bar{k}l \rightarrow +\infty} pdf_{K,2}(k) = pdf_{K,1}(k) = f(k)$. From the comparison of statistical errors obtained with $\phi = 10^{-2}$ and $\phi = 10^{-1}$ with those obtained for monochromatic simulations, it may be concluded that this pdf choice is well adapted to the physics of high optical thickness gaseous radiative exchanges. The additional spectral dimension is indeed only responsible of a factor 2 or 3 increase (for the same number of sampling events) of the statistical error, which means that $f(k)$ is a realistic model of the contribution of k in the $[0, +\infty[$ interval.

Observations are quite different in the small to moderate optical thickness ranges. Under such conditions, when using $pdf_{K,1}(k) = f(k)$ for k -sampling, the additional spectral dimension may induce as high as a two orders of magnitude increase of the statistical error, which means that $f(k)$ is a poor model of the contribution of k to radiative exchanges in the optically thin limit. It is the object of $pdf_{K,2}(k)$ to try to better model these k -contributions as functions of system optical thickness, which appears to be successful in the present test case. Similar observations were made in [21] for a wide range of combustion configurations, but we should emphasize that this pdf choice should receive some critical attention when considering distinct configuration types.

4. Conclusion

In this paper we presented a MC method that overcomes the difficulties encountered by classical MC methods when computing radiative transfers in optically thick media. In order to develop this method, we made a permanent link between the various MC algorithms, the corresponding integral equations and the corresponding statistical errors. Analytic expressions of these errors allowed us to formalize the interpretation of general algorithmic properties.

We first considered the computation of the energy emitted by a volume of participating media in a simple one-dimensional case. For current MC algorithms, we showed a monotonic increase of statistical error with optical thickness. The reason was identified as the random sampling of emission positions, which is uniform over the volume for classical MC methods. A new sampling procedure was designed that closely combines the generation of emission angles and emission positions in order to optimize the computation of the energy emitted by the volume. It takes into account the continuous change of the distribution emission directions at volume boundaries, which is isotropic when the medium is thin, and is lambertian when the medium is thick. It also favors emission positions close to the volume boundaries in such a way that there is again a continuous change of the sampling distribution of emission positions from a uniform distribution in the optically thin limit to an opaque surface-like emission in the optically thick limit.

For this first simple case, the new algorithm dramatically changes the behavior of the MC integration: the error now decreases when optical thickness increases. The reason is that when the medium is optically thin, the temperature and the optical properties have to be sampled inside the whole volume. But when the optical thickness is very high, the energy emitted by the volume is perfectly known and corresponds to the energy emitted by an equivalent black surface whose temperature is the temperature of the edge of the medium. Our algorithm takes advantage of this property and thus a few photons are enough to sample this edge.

Our algorithm was defined in order to optimize the computation of the energy emitted by a volume of participating media. Nevertheless one is often more concerned with computing the energy budget of a volume and of determining the distribution of corresponding internal radiative sources or loss. We therefore computed radiative budgets for various test profiles. Our method appears to be more accurate than previous MC algorithms, and overall we demonstrated that, with a constant number of sampling events, the relative statistical errors of estimated radiative budgets first increases slowly with optical thickness and finally reaches an asymptotic value for optically very thick configurations. The MC algorithm therefore remains efficient even for very high optical thicknesses.

We next considered the question of the required additional spectral integration when the medium is a gas with a separated line spectrum. We used a k -distribution approach based on the Malkmus narrow band statistical model. The first straightforward algorithm was to sample the absorption coefficient according to the k -distribution function. This method is far from being the most efficient but still produces acceptable results. For a given accuracy, the required number of sampling events is almost independent of optical thickness and is comparable to the number of sampling events required in the monochromatic case in the optically thick limit. This is consistent with the fact that within a narrow band, for separated line spectra, the absorption coefficient varies over a few orders of magnitude and thus the optically thick limit is always reached in some spectral regions. The design of a more adequate k -sampling procedure was the next step. Based on an empirical hypothesis, we showed that significant improvements can be obtained for low and intermediate optical thicknesses. Nevertheless a general methodology does not currently exist and further investigations are needed.

Acknowledgements

We are grateful to Professor J. Taine and A. Soufiani (EMZC/Ecole Centrale, Paris) for providing narrow band spectroscopic data bank and for valuable discussions about this work.

Appendix A

The radiative power emitted and exiting from a volume V_i may be expressed as

$$F = \int_{V_i} dV(\vec{e}) \int_{4\pi} d\omega(\vec{u}) k \exp(-k\|\vec{x}_1 - \vec{e}\|) B(\vec{e}),$$

where \vec{x}_1 is the location of the first encounter with V_i 's envelope, starting from \vec{e} in the direction \vec{u} . Computing this multiple integral using a standard MC algorithm, a uniform pdf is chosen for emission position random generation ($p_V(\vec{e}) = 1/V_i$) and an isotropic pdf for emission direction ($p_\Omega(\vec{u}) = 1/4\pi$) which leads to the following reformulation:

$$F = \int_{V_i} dV(\vec{e}) p_V(\vec{e}) \int_{4\pi} d\omega(\vec{u}) p_\Omega(\vec{u}) w(\vec{e}, \vec{u})$$

with

$$w(\vec{e}, \vec{u}) = 4\pi k V_i \exp(-k\|\vec{x}_1 - \vec{e}\|) B(\vec{e}).$$

Another formulation may be retained that leads to the basis of the MC algorithm detailed in the text. In this formulation, the total exiting flux is obtained by integrating surface fluxes over V_i 's envelope:

$$F = \int_{\mathcal{S}_i} ds(\vec{x}_1) \int_{2\pi} d\omega(\vec{u}) \int_0^{\|\vec{x}_2 - \vec{x}_1\|} d\sigma k \exp(-k\sigma)(\vec{u} \cdot \vec{n}_1) B(\vec{e}).$$

Introducing the proposed surface, angular and line pdf's, F may be written:

$$F = \int_{\mathcal{S}_i} ds(\vec{x}_1) p_S(\vec{x}_1) \int_{2\pi} d\omega(\vec{u}) p_{\Omega,a}(\vec{u}; \vec{n}_1, kL) \int_0^{\|\vec{x}_2 - \vec{x}_1\|} d\sigma p_{\Sigma}(\sigma) w(\vec{x}_1, \vec{u}, \sigma)$$

with

$$w(\vec{x}_1, \vec{u}, \sigma) = \pi \mathcal{S}_i [1 - \exp(-k\|\vec{x}_2 - \vec{x}_1\|)] \frac{p_{\Omega,l}(\vec{u}; \vec{n}_1)}{p_{\Omega,a}(\vec{u}; \vec{n}_1, kL)} B(\vec{e})$$

leading to Eq. (9).

In case of complex discretizations, the envelope \mathcal{S}_i may be difficult to handle and an alternative algorithm may be preferred that is based on the following formulation, in which the integration over \mathcal{S}_i is transformed into an integration over any convex closed surface $\mathcal{S}_{i,c}$ surrounding V_i (see Fig. 3b):

$$F = \int_{\mathcal{S}_{i,c}} ds(\vec{x}_0) \int_{2\pi} d\omega(\vec{u}) \sum_{l=1}^m \int_0^{\|\vec{x}_{2l} - \vec{x}_{2l-1}\|} d\sigma_l k \exp(-k\sigma_l)(\vec{u} \cdot \vec{n}_0) B(\vec{e}_l),$$

where \vec{n}_0 is the unit vector normal to $\mathcal{S}_{i,c}$ at \vec{x}_0 , the positions $\vec{x}_1, \dots, \vec{x}_{2m}$ are the successive locations of \mathcal{S}_i 's encounters starting from \vec{x}_0 in the direction $-\vec{u}$ and \vec{e}_l is defined as $\vec{e}_l = \vec{x}_{2l-1} - \sigma_l \vec{u}$.

Introducing the same surface, angular and line pdf's as above and introducing an arbitrary set of discrete probabilities P_1, \dots, P_m (corresponding to the discrete sum that appears in this last formulation choice) leads to

$$F = \int_{\mathcal{S}_{i,c}} ds(\vec{x}_0) p_S(\vec{x}_0) \int_{2\pi} d\omega(\vec{u}) p_{\Omega,a}(\vec{u}; \vec{n}_0, kL) \sum_{l=1}^m P_l \int_0^{\|\vec{x}_{2l} - \vec{x}_{2l-1}\|} d\sigma_l p_{\Sigma_l}(\sigma_l) w(\vec{x}_0, \vec{u}, l, \sigma_l)$$

with

$$p_S(\vec{x}_0) = \frac{1}{\mathcal{S}_{i,c}}, \quad p_{\Sigma_l}(\sigma_l) = \frac{k \exp(-k\sigma_l)}{1 - \exp(-k\|\vec{x}_{2l} - \vec{x}_{2l-1}\|)}$$

and

$$w(\vec{x}_0, \vec{u}, l, \sigma_l) = \frac{1}{P_l} \pi \mathcal{S}_{i,c} [1 - \exp(-k\|\vec{x}_{2l} - \vec{x}_{2l-1}\|)] \frac{p_{\Omega,l}(\vec{u}; \vec{n}_0)}{p_{\Omega,a}(\vec{u}; \vec{n}_0, kL)} B(\vec{e}_l).$$

The corresponding algorithm is very similar to the algorithm detailed in Sections 2 and 3. A position is generated uniformly on the convex surface and an outward direction is generated around the normal. These positions and directions define a finite number m of emission segments within V_i among which one is randomly chosen according to P_1, \dots, P_m . Finally the emission position is randomly generated along this segment according to an exponential pdf. We used such an alternative procedure practically when dealing with cylindrical configurations in which non-convex annulus grids are encountered [21].

References

- [1] Howell JR. Application of Monte Carlo to heat transfer problems. *Adv Heat Transfer* 1969;5:1–54.
- [2] Hammersley JM, Hanoscomb DS. *Les méthodes de Monte Carlo*. 1967.
- [3] Howell JR. The Monte Carlo method in radiative transfer. *J Heat Transfer* 1998;120:547–60.
- [4] Farmer JT, Howell JR. Hybrid Monte Carlo/diffusion method for enhanced solution of radiative transfer in optically thick non-gray media. In: Bayazitoglu Y, et al., editors. *Radiative transfer: current research*, vol. 276. New York: ASME, 1994. p. 203–12.
- [5] Farmer JT, Howell JR. Comparison of Monte Carlo strategies for radiative transfer in participating media. *Adv Heat Transfer* 1998;31:333–429.
- [6] Cherkaoui M, Dufresne J-L, Fournier R, Grandpeix J-Y, Lahellec A. Monte Carlo simulation of radiation in gases with a narrow-band model and a net-exchange formulation. *J Heat Transfer* 1996;118:401–7.
- [7] Farmer JT, Howell JR. Monte Carlo algorithms for predicting radiative heat transport in optically thick participating media. In *Proceedings of the 10th International Heat Transfer Conference*, vol. 2. Brighton, 1994. p. 37–42.
- [8] Surzhikov ST, Howell J. Monte Carlo simulation of radiation in scattering volumes with line structure. *AIAA J of Thermophys Heat Transfer* 1998;12:278–81.
- [9] Cherkaoui M, Dufresne J-L, Fournier R, Grandpeix J-Y, Lahellec A. Radiative net exchange formulation within one-dimensional gas enclosures with reflective surfaces. *J Heat Transfer* 1998;120:275–8.
- [10] Malkmus W. Random lorentz band model with exponential-tailed s-1 line-intensity distribution function. *J Opt Soc Am* 1967;57:323–9.
- [11] Domoto GA. Frequency integration for radiative transfer problems involving homogeneous non-gray gases: the inverse transmission function. *JQSRT* 1974;14:935–42.
- [12] Dufresne J-L, Fournier R, Grandpeix J-Y. Inverse gaussian k -distributions. *JQSRT* 1999;61:433–41.
- [13] Goody RM. *Atmospheric radiation theoretical basis*. 1989.
- [14] Goody RM. The correlated k method for radiation calculations in nonhomogeneous atmospheres. *JQSRT* 1989;42:539–50.
- [15] Gerstell MF. Obtaining the cumulative k -distribution of a gas mixture from those of its components. *JQSRT* 1993;49:15–38.
- [16] Lacis AA, Oinas V. A description of the correlated- k distribution method for modeling nongray gaseous absorption, thermal emission and multiple scattering in vertically inhomogeneous atmospheres. *J Geophys Res* 1991;96:9027–63.
- [17] Taine J, Soufiani A. Gas irradiative properties: From spectroscopic data to approximate models. *Adv Heat Transfer* 1998;33:295–414.
- [18] Modest MF. The Monte Carlo method applied to gases with spectral line structure. *Num Heat Transfer, Part B* 1992;22:273–84.
- [19] Dufresne J-L, Fournier R, Grandpeix J-Y. Méthode de Monte Carlo par échanges pour le calcul des bilans radiatifs au sein d'une cavité 2d remplie de gaz. *CR Acad Sci* 1998;326:33–8.
- [20] Tessé L, Dupoirieux F, Taine J, Zamuner B. Simulation of radiative transfer in real gases using a Monte-Carlo method and a correlated- k approach. *Int J Heat Mass Transfer*. 2002, submitted for publication.
- [21] de Guilhem de Lataillade A. Modélisation détaillée des transferts radiatifs et couplage avec la cinétique chimique dans des systèmes en combustion. Thèse INP Toulouse no. 1775, 2001.